



Unexpected reactivity resulting from modifications of the ligand periphery: Synthesis, structure, and spectroscopic properties of iron complexes of new tripodal N-heterocyclic carbene (NHC) ligands

Carola S. Vogel, Frank W. Heinemann, Marat M. Khusniyarov, Karsten Meyer*

Department of Chemistry and Pharmacy, Inorganic Chemistry, University Erlangen-Nuremberg, Egerlandstraße 1, D-91058 Erlangen, Germany

ARTICLE INFO

Article history:

Available online 17 August 2010

Dedicated to Prof. Arnold L. Rheingold

Keywords:

Iron
Carbene ligands
C–H bond activation
Cyclometallation
Crystal structure determination

ABSTRACT

The chelating ligand tris-[2-(3-aryl-imidazol-2-ylidene)ethyl]amine (TIMEN^R, R = aryl = 2,6-xylyl (xyl), mesityl (mes)) has provided access to reactive transition metal complexes. Here, two new tripodal N-heterocyclic carbene ligands of the TIMEN^R system (R = aryl = tolyl (tol), 3,5-xylyl (3,5xyl)), featuring sterically less demanding aryl substituents were synthesized. With these ligands, Fe(II) precursor complexes could be obtained, namely [(TIMEN^{tol})Fe](BF₄)₂ (**3**) and [(TIMEN^{3,5xyl})Fe](CH₃CN)(PF₆)₂ (**7**), which showed unexpected reactivity upon reduction. Treatment of the compounds with sodium amalgam yield the tris- and bis-metallated products, [(TIMEN^{tol})Fe] (**4**) and [(TIMEN^{3,5xyl})Fe] (**8**), respectively. While the Fe(III) complex **4** is relatively inert towards oxygen, the Fe(II) complex **8** is prone to oxidation. This oxidation of **8** can readily be observed in chlorinated solvents, producing the Fe(III) complex [(TIMEN^{3,5xyl})Fe](PF₆) (**9**). All new ligand imidazolium precursors and metal complexes were characterized by single crystal X-ray structure determination.

© 2010 Elsevier B.V. All rights reserved.

1. Introduction

Coordinatively unsaturated, electron-rich metal complexes have proven to be powerful species for small molecule activation and functionalization [1]. Due to their σ -donor and π -accepting properties [2–4], N-heterocyclic carbene (NHC) ligands are particularly suitable for the synthesis of a variety of low to high-valent metal complexes; thus, perfectly suitable to act as supporting ligands for small molecule activation at reactive coordination complexes [5]. The steric bulk of NHC ligands is highly tunable and often the ligands can be conveniently synthesized. The anchoring unit of polydentate NHC systems provides the chelators with additional electronic and structural flexibility. It could be shown that sterically encumbering tripodal ligands of tris-[2-(3-aryl-imidazol-2-ylidene)ethyl]amine (TIMEN^R, with R = aryl = 2,6-xylyl (xyl), mesityl (mes)) create a trigonal platform for metal ions that enables the coordination and activation of small molecules of industrial and biological importance in a protective cylindrical cavity, such as dinitrogen [6].

An iron active center with an iron nitride moiety has recently been suggested to be present at the site of biological nitrogen reduction [7] and significant progress in the synthesis and spectroscopic elucidation of iron imide, Fe=NR, and nitride species, Fe≡N,

was achieved [8]. The first X-ray crystal structure determination of a discrete iron nitride complex, [(TIMEN^R)Fe(N)]⁺, was recently accomplished after photolysis of an iron-azide complex stabilized by the N-anchored tris(carbene) ligand TIMEN^R [9]. Shortly after this, the second X-ray crystallographic characterization of an iron nitride complex with a closely related borate-anchored tris(carbene) ligand was reported by Smith and co-workers, namely [(PhB^{tbu}Im)Fe(N)], with [(PhB^{tbu}Im) = phenyltris(1-*tert*-butylimidazol-2-ylidene)borate(1-)] [10], reflecting the potential of carbene based ligand systems, not only for the stabilization but for the synthesis of reactive iron nitride complexes as well. Interestingly, the reactivity of the N-anchored Fe≡N appears to be fundamentally different compared to the B-anchored system. While the B-anchored Fe≡N system shows reactivity towards a number of substrates, like the triphenylmethyl radical or TEMPO-H (1-hydroxy-2,2,6,6-tetramethyl-piperidine), the N-anchored Fe≡N complexes are remarkably inert towards the same substrates [11]. This observed difference in reactivity might be a result of the individual electronic and geometric structures of these two Fe(IV) systems. While the N-anchored complex is best described as trigonal pyramidal, the iron ion in the B-based Fe≡N is tetrahedrally coordinated. Additionally, the steric demand of the two NHC tripods is markedly different. In contrast to the relatively accessible Fe≡N unit in [(PhB^{tbu}Im)Fe(N)], the nitride functionality in [(TIMEN^R)Fe(N)]⁺ is situated in a deep cylindrical cavity with no side-access for substrates.

* Corresponding author.

E-mail address: karsten.meyer@chemie.uni-erlangen.de (K. Meyer).

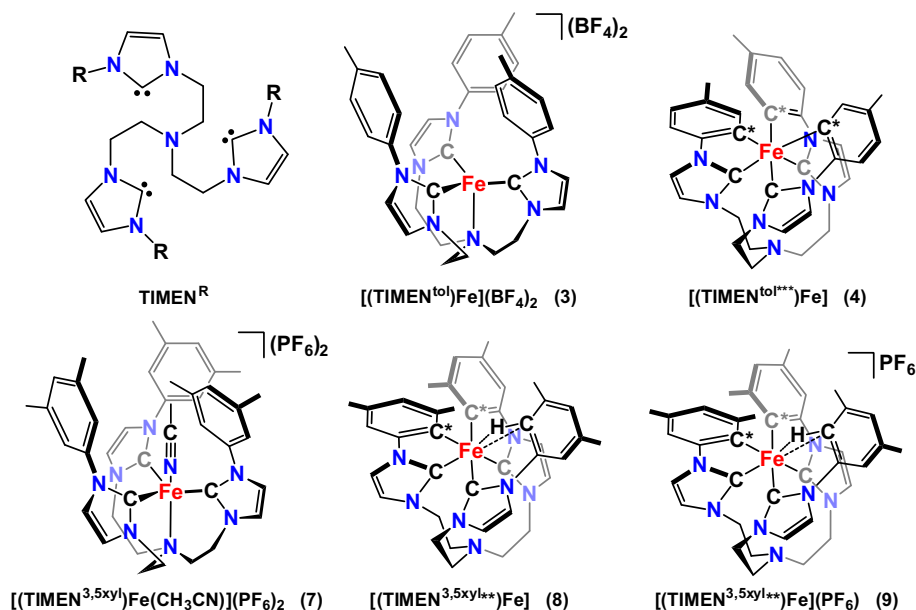


Chart 1. Overview of the tripodal TIMEN^R ligand and its iron complexes.

In order to synthesize N-anchored Fe≡N complexes with increased reactivity, we started to modify our NHC systems by varying the steric demand of the aryl substituents. Here, we present the synthesis and characterization of two new N-anchored NHC ligands of the TIMEN^R system, namely the tolyl and the 3,5-xylyl derivatives [TIMEN^{tol}] and [TIMEN^{3,5xyl}]. During the synthesis of the corresponding iron complexes, unexpected reactions were observed resulting in the here presented series of new four, five, and six-coordinate iron complexes (see Chart 1). The synthesis, spectroscopic, and X-ray structural characterization of the iron complexes [(TIMEN^{tol})Fe](BF₄)₂ (**3**), [(TIMEN^{tol*})Fe] (**4**), [(TIMEN^{3,5xyl})Fe(CH₃CN)](PF₆)₂ (**7**), [(TIMEN^{3,5xyl*})Fe] (**8**) and [(TIMEN^{3,5xyl*})Fe](PF₆) (**9**) is presented. The electronic structures of **4**, **8**, and **9** were examined by density functional theory (DFT) calculations and are presented as well.

2. Experimental

2.1. General considerations

All air- and moisture-sensitive experiments were performed under dry nitrogen atmosphere using standard Schlenk line techniques or an MBraun inert-gas glovebox containing an atmosphere of purified dinitrogen. Anhydrous iron(II) chloride, 99.9%, was purchased from Aldrich and used as received. Sodium tetraphenylborate, potassium *tert*-butoxide, and sodium *tert*-butoxide were purchased from ACROS and were used without further purification. Solvents were purified using a two-column solid-state purification system (Glasscontour System, Irvine, CA) and transferred to the glove box without exposure to air. NMR solvents were obtained packaged under argon and stored over activated molecular sieves and sodium (where appropriate) prior to use. Tris-(2-chloroethyl)amine, 1-(3,5-xylyl)imidazole, and 1-(tolyl)imidazole were synthesized according to literature [12,13]. Elemental analysis were performed at the Analytical Laboratories at the Friedrich-Alexander-University Erlangen-Nuremberg (Erlangen, Germany). Due to poor solubility, limited stability, and difficulties in separation of the reactants during work-up of some of the compounds, certain routine analytical methods could not be applied. Yields were calculated and noted where possible. All compounds were

characterized by single crystal X-ray structure determination with crystals being representative for the bulk sample.

2.2. Spectroscopic methods

¹H NMR spectra were recorded on JEOL 270 and 400 MHz instruments, operating at respective frequencies of 269.714 and 400.178 MHz with a probe temperature of 23 °C. ¹³C NMR spectra were recorded on JEOL 270 and 400 MHz instruments, operating at respective frequencies of 67.82 and 100.624 MHz with a probe temperature of 23 °C. Chemical shifts were reported in ppm relative to the peak of SiMe₄ using ¹H (residual) chemical shifts of the solvent as a secondary standard.

⁵⁷Fe Mössbauer spectra were recorded on a WissEl Mössbauer spectrometer (MRG-500) at 77 K in constant acceleration mode. ⁵⁷Co/Rh was used as the radiation source. WinNormos for Igor Pro software was used for the quantitative evaluation of the spectral parameters (least-squares fitting to Lorentzian peaks). The minimum experimental line widths were 0.23 mm s⁻¹. The temperature of the samples was controlled by an MBBC-HE0106 MÖSSBAUER He/N₂ cryostat within an accuracy of ±0.3 K. Isomer shifts were determined relative to α-iron at 298 K.

EPR measurements were performed in quartz tubes with J. Young valves. Frozen solution EPR spectra were recorded on a JEOL continuous wave spectrometer JESFA200 equipped with an X-band Gunn diode oscillator bridge, a cylindrical mode cavity, and a helium cryostat. For all samples, a modulation frequency of 100 kHz and a time constant of 0.1 s were employed. All spectra were obtained on freshly prepared solutions of 1–10 mM compound in acetonitrile.

2.3. X-ray crystal structure determinations

Colorless plates of [H₃TIMEN^{tol}](CF₃SO₃)₃ (**1**(CF₃SO₃)₃) were grown by layering an *n*-pentane solution of the corresponding imidazolium salt with diethyl ether. Colorless plates of [(TIMEN^{tol})Fe](BF₄)₂ · 0.8 Et₂O (**3** · 0.8 Et₂O) were obtained from a solution of the complex in a mixture of acetonitrile and diethyl ether. Dark red needles of [(TIMEN^{tol*})Fe] · 2 THF (**4** · 2 THF) were grown from a THF solution of the complex at –37 °C. Colorless plates of

Table 1
Crystallographic data, data collection, and refinement details of $[\text{H}_3\text{TIMEN}^{\text{tol}}](\text{CF}_3\text{SO}_3)_3$ (**1** (CF_3SO_3)₃), $[(\text{TIMEN}^{\text{tol}})\text{Fe}](\text{BF}_4)_2 \cdot 0.8 \text{ Et}_2\text{O}$ (**3** · 0.8 Et₂O), and $[(\text{TIMEN}^{\text{tol***}})\text{Fe}] \cdot 2 \text{ THF}$ (**4** · 2 THF).

	1 (CF ₃ SO ₃) ₃ [H ₃ TIMEN ^{tol}](CF ₃ SO ₃) ₃	3 · 0.8 Et ₂ O [(TIMEN ^{tol})Fe](BF ₄) ₂ · 0.8 Et ₂ O	4 · 2 THF [(TIMEN ^{tol***})Fe] · 2 THF
Empirical formula	C ₃₉ H ₄₂ F ₉ N ₇ O ₉ S ₃	C _{39.2} H ₄₇ B ₂ F ₈ FeN ₇ O _{0.8}	C ₄₄ H ₅₂ FeN ₇ O ₂
Molecular weight	1019.98	858.51	766.78
Crystal size (mm ³)	0.37 × 0.11 × 0.10	0.24 × 0.18 × 0.07	0.20 × 0.10 × 0.08
T (K)	100	100	150
Crystal system	triclinic	monoclinic	triclinic
Space group	<i>P</i> $\bar{1}$ (no. 2)	<i>P</i> 2 ₁ / <i>c</i> (no. 14)	<i>P</i> $\bar{1}$ (no. 2)
<i>a</i> (Å)	10.2584(7)	14.761(2)	12.355(1)
<i>b</i> (Å)	12.483(2)	13.986(2)	13.3642(8)
<i>c</i> (Å)	19.679(2)	20.053(3)	13.7659(7)
α (°)	73.265(10)	90	106.685(4)
β (°)	84.479(8)	100.39(2)	90.960(5)
γ (°)	67.943(2)	90	116.281(5)
<i>V</i> (Å ³)	2236.4(5)	4071.9(9)	1924.7(2)
<i>Z</i>	2	4	2
ρ_{calc} (g/cm ³)	1.515	1.400	1.323
μ (mm ⁻¹)	0.265	0.448	0.440
<i>F</i> (0 0 0)	1052	1782	814
<i>T</i> _{min} ; <i>T</i> _{max}	0.897; 0.970	0.846; 0.970	0.842; 0.965
2 θ interval (°)	6.7 ≤ 2 θ ≤ 54.2	6.6 ≤ 2 θ ≤ 54.2	6.2 ≤ 2 θ ≤ 54.2
Collected reflections	66 332	85 162	53 280
Independent reflections (<i>R</i> _{int})	9846 (0.0441)	8955 (0.0667)	8478 (0.0371)
Observed reflections [<i>I</i> ≥ 2 σ (<i>I</i>)]	7902	7000	7410
No. refined parameters	671	637	536
<i>wR</i> ₂ (all data)	0.0900	0.1159	0.1223
<i>R</i> ₁ [<i>I</i> ≥ 2 σ (<i>I</i>)]	0.0366	0.0449	0.0428
Goodness of fit (GOF) on <i>F</i> ²	1.023	1.044	1.052
$\Delta\rho_{\text{max/min}}$	0.527/−0.358	0.495/−0.458	0.917/−0.587

$[\text{H}_3\text{TIMEN}^{3,5\text{xy1}}](\text{Cl})_3 \cdot \text{solv}$ (**5**(Cl)₃ · solv (solv = 0.9735 CHCl₃ · 2.125 H₂O)) precipitated at room temperature from a CHCl₃ solution of the hygroscopic imidazolium salt layered with diethyl ether. Brown irregular shaped crystals of $[(\text{TIMEN}^{3,5\text{xy1}})\text{Fe}](\text{CH}_3\text{CN})(\text{PF}_6)_2 \cdot 2 \text{ CH}_3\text{CN}$ (**7** · 2 CH₃CN) were obtained by slow diethyl ether diffusion into a layered acetonitrile solution of the complex. Dark red plates of $[(\text{TIMEN}^{3,5\text{xy1***}})\text{Fe}]$ (**8**) were grown from a THF/*n*-pentane mixture. Brown plates of $[(\text{TIMEN}^{3,5\text{xy1***}})\text{Fe}](\text{PF}_6) \cdot 0.6 \text{ THF} \cdot 0.4 \text{ CHCl}_3$ (**9** · 0.6 THF · 0.4 CHCl₃) were grown from a mixture of chloroform, dichloromethane and THF. For crystallographic data, data collection, and refinement details see Tables 1 and 2. Suitable single crystals of the compounds were embedded in protective perfluoropolyalkylether oil and quickly transferred to the cold nitrogen gas stream of the diffractometer. Intensity data were collected either on a Bruker–Nonius KappaCCD diffractometer (**1**(CF₃SO₃)₃, **3** · 0.8 Et₂O, **4** · 2 THF, **7** · 2 CH₃CN and **8**) using graphite monochromatized Mo K α radiation ($\lambda = 0.71073 \text{ \AA}$) or on a Bruker Kappa APEX2 Duo diffractometer (**5**(Cl)₃ · solv and **9** · 0.6 THF · 0.4 CHCl₃) equipped with an *I* μ S microsource and QUAZAR focusing optics using Mo K α radiation ($\lambda = 0.71073 \text{ \AA}$). Lorentz and polarization effects were taken into account during data reduction, semiempirical absorption corrections were performed on the basis of multiple scans using SADABS [14]. All structures were solved by direct methods and refined by full-matrix least-squares procedures on *F*² (with the exception of **5** · solv, which was refined in a block matrix) using SHELXTL NT 6.12 [15].

In $[\text{H}_3\text{TIMEN}^{\text{tol}}](\text{CF}_3\text{SO}_3)_3$ (**1**(CF₃SO₃)₃), one of the imidazolium rings is disordered. Two preferred orientations were refined resulting in occupancies of 86.9(3)% for atoms N2, N3, C1–C5 and 13.1(3)% for N2A, N3A, C1A–C5A. SIMU and ISOR restraints were applied. In $[(\text{TIMEN}^{\text{tol}})\text{Fe}](\text{BF}_4)_2 \cdot 0.8 \text{ Et}_2\text{O}$ (**3** · 0.8 Et₂O) both BF₄ anions are subjected to rotational disorder around one B–F bond. Two preferred orientations were refined each resulting in occupancies of 57(2) and 43(2)% for atoms F12–F14 and F12A–F14A, respectively and of 52(5) and 48(5)% for atoms F22–F24 and F22A–F24A, respectively. $[(\text{TIMEN}^{\text{tol***}})\text{Fe}] \cdot 2\text{THF}$ (**4** · 2THF) crystallizes with two molecules of THF per formula unit one of which is disordered showing two alternative orientations of 46.4(7) and 53.6(7)%

occupancy for O200–C204 and O210–C214, respectively. SIMU, ISOR and SAME restraints were applied in the refinement of the disorder. The asymmetric unit of $[\text{H}_3\text{TIMEN}^{3,5\text{xy1}}](\text{Cl})_3 \cdot \text{solv}$ (**5**(Cl)₃ · solv) contains a total of four independent molecules of the imidazolium salt, 3.75 molecules of CHCl₃ and 8.5 molecules of solvent water. In one of the imidazolium cations one of the three ligand arms is disordered. Two alternative positions were refined resulting in site occupancies of 81.4(2) and 18.6(2)% for the atoms N306, N307, C311–C315, C332–C339 and N406, N407, C411–C415, C432–C439, respectively. This disorder also affects some of the CHCl₃ solvate molecules while other solvate molecules are occupied by approximately 50% or 75%. SIMU, ISOR, DFIX, FLAT, and SAME restraints were applied in the refinement of **5**(Cl)₃ · solv. In $[(\text{TIMEN}^{3,5\text{xy1}})\text{Fe}](\text{CH}_3\text{CN})(\text{PF}_6)_2 \cdot 2 \text{ CH}_3\text{CN}$ (**7** · 2 CH₃CN), one of the PF₆ anions is disordered. Two alternative orientations were refined resulting in occupancies of 61.6(6) and 38.9(6)% for atoms P2–F26 and P2A–F26A, respectively. In $[(\text{TIMEN}^{3,5\text{xy1***}})\text{Fe}](\text{PF}_6) \cdot 0.6 \text{ THF} \cdot 0.4 \text{ CHCl}_3$ (**9** · 0.6 THF · 0.4 CHCl₃), one of the PF₆ anions is subjected to rotational disorder in the equatorial plane. Two alternative orientations were refined resulting in occupancies of 59.8(6)% and 40.2(6)% for atoms F13–F16 and F13A–F16A, respectively. Compound **9** · 0.6 THF · 0.4 CHCl₃ crystallizes with a mixture of solvent molecules (0.6CHCl₃ and 0.4THF) which share a common crystallographic site. SIMU, ISOR, and SAME restraints were applied in the refinement.

In the computations of the crystal structure determinations of compounds **1** to **9**, all non-hydrogen atoms were refined with anisotropic displacement parameters. All hydrogen atoms were placed in positions of optimized geometry, their isotropic displacement parameters were tied to those of the corresponding carrier atoms by a factor of either 1.2 or 1.5.

2.4. Syntheses and characterization

2.4.1. $[\text{H}_3\text{TIMEN}^{\text{tol}}](\text{BF}_4)_3$ (**1**(BF₄)₃)

A 100 mL flask was charged with tris-(2-chloroethyl)amine (4.06 g, 19.86 mmol) and 1-(tolyl)imidazole (9.43 g, 59.59 mmol), the mixture was heated to 150 °C for 2 days. The resulting brown

Table 2

Crystallographic data, data collection, and refinement details of $[\text{H}_3\text{TIMEN}^{3,5\text{xy}1}](\text{Cl})_3 \cdot \text{solv}$ ($5(\text{Cl})_3 \cdot \text{solv}$), $[(\text{TIMEN}^{3,5\text{xy}1})\text{Fe}(\text{CH}_3\text{CN})](\text{PF}_6)_2 \cdot 2 \text{CH}_3\text{CN}$ ($7 \cdot 2 \text{CH}_3\text{CN}$), $[(\text{TIMEN}^{3,5\text{xy}1})\text{Fe}]$ (**8**), and $[(\text{TIMEN}^{3,5\text{xy}1})\text{Fe}](\text{PF}_6) \cdot 0.6 \text{THF} \cdot 0.4 \text{CHCl}_3$ (**9** · 0.6 THF · 0.4 CHCl₃).

	$5(\text{Cl})_3 \cdot \text{solv}$ [$\text{H}_3\text{TIMEN}^{3,5\text{xy}1}$] (Cl) ₃ · solv	$7 \cdot 2 \text{CH}_3\text{CN}$ [$(\text{TIMEN}^{3,5\text{xy}1})\text{Fe}$ - (CH ₃ CN)](PF ₆) ₂ · 2 CH ₃ CN	8 [($\text{TIMEN}^{3,5\text{xy}1}$)Fe]	9 · 0.6 THF · 0.4 CHCl ₃ [($\text{TIMEN}^{3,5\text{xy}1}$)Fe](PF ₆) · 0.6 THF · 0.4 CHCl ₃
Empirical formula	C _{39.9375} H _{53.1875} Cl _{5.8125} N ₇ O _{2.125}	C ₄₅ H ₅₄ F ₁₂ FeN ₁₀ P ₂	C ₃₉ H ₄₃ FeN ₇	C _{41.8} H _{48.2} Cl _{1.2} F ₆ FeN ₇ O _{0.6} P
Molecular weight	871.39	1080.77	665.65	901.63
Crystal size (mm ³)	0.28 × 0.16 × 0.04	0.50 × 0.23 × 0.18	0.24 × 0.08 × 0.08	0.20 × 0.06 × 0.02
T (K)	100	150	150	100
Crystal system	triclinic	triclinic	triclinic	monoclinic
Space group	<i>P</i> $\bar{1}$ (no. 2)	<i>P</i> $\bar{1}$ (no. 2)	<i>P</i> $\bar{1}$ (no. 2)	<i>P</i> $\bar{1}$ (no. 2)
<i>a</i> (Å)	17.660(4)	11.488(2)	11.5632(7)	14.001(2)
<i>b</i> (Å)	21.259(5)	14.968(2)	11.9611(7)	13.587(2)
<i>c</i> (Å)	26.505(6)	15.908(2)	12.3184(9)	23.134(4)
α (°)	106.629(4)	74.453(7)	81.472(5)	90
β (°)	104.166(4)	88.036(8)	71.432(5)	102.443(3)
γ (°)	94.311(4)	70.889(7)	82.705(5)	90
<i>V</i> (Å ³)	9131(4)	2485.7(4)	1591.4(2)	4297(2)
<i>Z</i>	8	2	2	4
ρ_{calc} (g/cm ³)	1.341	1.444	1.389	1.394
μ (mm ⁻¹)	0.406	0.457	0.516	0.530
<i>F</i> (0 0 0)	3661	1116	704	1873
<i>T</i> _{min} ; <i>T</i> _{max}	0.665; 0.746	0.739; 0.921	0.818; 0.960	0.506; 0.421
2 θ interval (°)	6.0 ≤ 2 θ ≤ 51.4	6.5 ≤ 2 θ ≤ 54.2	6.7 ≤ 2 θ ≤ 54.2	5.1 ≤ 2 θ ≤ 54.2
Collected reflections	134 232	70 427	45 758	33 178
Independent reflections (<i>R</i> _{int})	34 579 (0.0905)	10 940 (0.0725)	7010 (0.0711)	9448 (0.0697)
Observed reflections [<i>I</i> ≥ 2 σ (<i>I</i>)]	17 923	8332	5529	6073
No. refined parameters	2248	704	430	612
<i>wR</i> ₂ (all data)	0.2667	0.1269	0.0901	0.1285
<i>R</i> ₁ [<i>I</i> ≥ 2 σ (<i>I</i>)]	0.0892	0.0467	0.0397	0.0506
Goodness of fit (GOF) on <i>F</i> ²	1.341	1.039	1.025	1.010
$\Delta\rho_{\text{max/min}}$	1.811/−1.203	0.696/−0.577	0.368/−0.369	0.506/−0.421

solid was dissolved in 20 mL of methanol and the hygroscopic chloride salt was converted to the corresponding stable tetrafluoroborate salt, $[\text{H}_3\text{TIMEN}^{\text{tol}}](\text{BF}_4)_3$, by addition of a solution of NaBF₄ (6.41 g, 60.00 mmol) in 50 mL of methanol. The tetrafluoroborate salt precipitated immediately, was collected by filtration, washed with methanol and diethyl ether, and dried *in vacuo*.

Yield, 9.19 g (11.02 mmol, 56%). *Anal. Calc.* for C₃₆H₄₄B₃F₁₂N₇O: C, 50.80; H, 5.21; N, 11.52. Found: C, 50.90; H, 5.08; N, 11.18%. ¹H NMR (270 MHz, RT, DMSO-*d*₆): δ [ppm] = 9.66 (s, 3H), 8.16 (d, 3H, ³*J* = 1.5 Hz), 7.85 (d, 3H, ³*J* = 1.5 Hz), 7.54 (d, 6H, ³*J* = 8.6 Hz), 7.37 (d, 6H, ³*J* = 8.0 Hz), 4.36 (t, 6H, ³*J* = 6.5 Hz), 3.15 (s, 6H, ³*J* = 6.8 Hz), 2.38 (s, 9H). ¹³C{¹H} NMR (100 MHz, RT, DMSO-*d*₆): δ [ppm] = 214.93 (3C), 135.17 (3C), 132.17 (3C), 130.52 (6C), 123.38 (3C), 121.32 (6C), 120.77 (3C), 51.32 (3C), 46.13 (3C), 20.57 (3C).

2.4.2. $[(\text{TIMEN}^{\text{tol}})]$ (**2**)

A solution of potassium *tert*-butoxide (340 mg, 3.03 mmol) in 10 mL THF was added to a suspension of $[\text{H}_3\text{TIMEN}^{\text{tol}}](\text{BF}_4)_3$ (722 mg, 0.87 mmol) in 5 mL of THF and stirred for 3 h. The solution was then evaporated to dryness and the solid residue was dissolved in 15 mL of diethyl ether. The resulting solution was filtered through celite and evaporated to dryness *in vacuo*.

¹H NMR (270 MHz, RT, benzene-*d*₆): δ [ppm] = 7.74 (d, 6H, ³*J* = 8.5 Hz), 6.90 (d, 6H, ³*J* = 8.5 Hz), 6.82 (d, 3H, ³*J* = 2.1 Hz), 6.43 (d, 3H, ³*J* = 2.1 Hz), 3.87 (t, 6H, ³*J* = 6.2 Hz), 2.70 (t, 6H, ³*J* = 6.2 Hz), 2.00 (s, 9H). ¹³C{¹H} NMR (100.5 MHz, RT, benzene-*d*₆): δ [ppm] = 214.61 (3C), 140.71 (3C), 135.28 (3C), 129.88 (6C), 121.22 (3C), 120.91 (6C), 116.55 (3C), 56.41 (3C), 49.73 (3C), 20.71 (3C).

2.4.3. $[(\text{TIMEN}^{\text{tol}})\text{Fe}](\text{BF}_4)_2$ (**3**)

Method A: $[\text{H}_3\text{TIMEN}^{\text{tol}}](\text{BF}_4)_3$ (1000 mg, 1.21 mmol) and sodium *tert*-butoxide (400 mg, 1.21 mmol) in 15 mL THF were stirred for 2 h, filtered and added to a suspension of FeCl₂ (135 mg, 1.21 mmol) in 5 mL pyridine. The reaction mixture was allowed to stir overnight, during which time an off-white precipitate formed. The precipitate was collected by filtration, washed with pyridine, diethyl ether and *n*-pentane, and dried *in vacuo*.

Method B: A mixture of $[\text{H}_3\text{TIMEN}^{\text{tol}}](\text{BF}_4)_3$ (1000 mg, 1.21 mmol), sodium *tert*-butoxide (400 mg), NaBPh₄ (410 mg, 1.21 mmol) and FeCl₂ (135 mg, 1.21 mmol) in THF was allowed to stir overnight, during which time an off-white precipitate formed. The precipitate was collected by filtration, washed with THF, diethyl ether and *n*-pentane, yielding the crude product. Recrystallization can be achieved by dissolving the crude product in acetonitrile and layering with diethyl ether at room temperature.

Anal. Calc. for C₃₆H₃₉B₂F₈FeN₇: C, 54.10; H, 4.92; N, 12.27. Found: C, 53.69; H, 5.07; N, 12.29%. In the ¹H NMR spectrum, 11 signals are expected for the complex, four are observed; the remaining signals are likely shifted and broadened into the baseline due to the paramagnetism of the compound. ¹H NMR (270 MHz, RT, acetonitrile-*d*₃): δ [ppm] = −0.94, 10.61, 12.16, 14.59. Mößbauer parameters: δ = 0.51(1) mm s^{−1}, ΔE_Q = 1.54(1) mm s^{−1}, Γ_{FWHM} = 0.28(1) mm s^{−1}

2.4.4. $[(\text{TIMEN}^{\text{tol}})\text{Fe}]$ (**4**)

A solution of $[(\text{TIMEN}^{\text{tol}})\text{Fe}](\text{BF}_4)_2$ (155 mg, 0.19 mmol) in THF was stirred over an excess of sodium amalgam (3300 mg, Na 0.8 wt.%) overnight. The resulting red solution and precipitate were separated from the sodium amalgam with the help of a Pasteur pipette, the THF was removed and after addition of CHCl₃ the

resulting solution was filtered through celite. Removal of the solvent yields the crude product. Recrystallization can be achieved by dissolving the crude product in a mixture of CHCl_3 and benzene and cooling the filtered solution to -35°C .

EPR (acetonitrile, 7.1 K, 8.987523 GHz, ModWidth = 1.0 mT, Power = 1.00 mW) $g_{\parallel} = 2.29$, $g_{\perp} = 1.94$. Mößbauer parameters: $\delta = 0.03(1) \text{ mm s}^{-1}$, $\Delta E_Q = 2.37(1) \text{ mm s}^{-1}$, $\Gamma_{\text{FWHM}} = 0.26(1) \text{ mm s}^{-1}$.

2.4.5. $[\text{H}_3\text{TIMEN}^{3,5\text{xy}l}](\text{PF}_6)_3$ (**5**(PF_6)₃)

A 50 mL flask was charged with tris-(2-chloroethyl)amine (8.49 g, 41.50 mmol) and 1-(3,5-xylyl)imidazole (22.00 g, 128.00 mmol), the mixture was heated to 150°C for 2 days. The resulting brown solid was dissolved in 30 mL of methanol and the hygroscopic chloride salt was converted to the corresponding stable hexafluorophosphate salt, $[\text{H}_3\text{TIMEN}^{3,5\text{xy}l}](\text{PF}_6)_3$, by addition of a solution of NH_4PF_6 (22.00 g, 135.00 mmol) in 150 mL of methanol. The white hexafluorophosphate salt precipitated immediately, was collected by filtration, washed with methanol and diethyl ether, and the solid was dried *in vacuo*.

Yield, 28.39 g (27.00 mmol, 65%), ^1H NMR (400 MHz, RT, DMSO- d_6): δ [ppm] = 9.72 (s, 3H), 8.16 (s, 3H), 7.88 (s, 3H), 7.34 (s, 6H), 7.25 (s, 3H), 4.39 (t, 6H, $^3J = 7.48 \text{ Hz}$), 3.20 (t, 6H, $^3J = 7.48 \text{ Hz}$), 2.35 (s, 18H). $^{13}\text{C}\{^1\text{H}\}$ NMR (100.5 MHz, RT, DMSO- d_6): δ [ppm] = 139.80 (6C), 135.12 (3C), 134.29 (3C), 130.92 (3C), 123.26 (3C), 120.60 (3C), 118.83 (6C), 50.85 (3C), 48.02 (3C), 20.56 (6C).

2.4.6. $[\text{TIMEN}^{3,5\text{xy}l}]$ (**6**)

A solution of potassium *tert*-butoxide (0.33 g, 2.95 mmol) in THF was added to a suspension of $[\text{H}_3\text{TIMEN}^{3,5\text{xy}l}](\text{PF}_6)_3$ (1.00 g, 0.95 mmol) in 5 mL of THF and stirred for 1 h. The solution was then evaporated to dryness and the solid residue was dissolved in 15 mL of diethyl ether. The resulting solution was filtered through celite and the filtrate was evaporated to dryness *in vacuo*.

^1H NMR (270 MHz, RT, benzene- d_6): $\delta = 7.54$ (s, 6H), 6.88 (m, 3H), 6.67 (m, 6H), 6.63 (d, 3H, $^3J = 1.32 \text{ Hz}$), 3.99 (t, 6H, $^3J = 6.24 \text{ Hz}$), 2.84 (t, 6H, $J = 6.24 \text{ Hz}$), 2.12 ppm (s, 18H). $^{13}\text{C}\{^1\text{H}\}$ NMR (100.5 MHz, RT, benzene- d_6): $\delta = 212.70$ (3C), 142.46 (3C), 138.55 (6C), 128.33 (3C), 121.07 (3C), 118.95 (6C), 116.48 (3C), 56.15 (3C), 49.38 (3C), 21.02 (6C) ppm.

2.4.7. $[(\text{TIMEN}^{3,5\text{xy}l})\text{Fe}(\text{CH}_3\text{CN})](\text{PF}_6)_2$ (**7**)

$[\text{H}_3\text{TIMEN}^{3,5\text{xy}l}](\text{PF}_6)_3$ (1.00 g, 0.95 mmol) and potassium *tert*-butoxide (0.33 g, 2.95 mmol) in 15 mL THF were stirred for 2 h, filtered and added to a suspension of FeCl_2 (0.12 g, 0.95 mmol) in 5 mL pyridine. The reaction mixture was allowed to stir overnight, during which time an off-white precipitate formed. The precipitate was collected by filtration, washed with pyridine, diethyl ether and *n*-pentane, and dried *in vacuo*. Recrystallization of $[(\text{TIMEN}^{3,5\text{xy}l})\text{Fe}](\text{PF}_6)_2$ from a solvent mixture of acetonitrile and diethyl ether yielded the compound $[(\text{TIMEN}^{3,5\text{xy}l})\text{Fe}(\text{CH}_3\text{CN})](\text{PF}_6)_2$ with a coordinated acetonitrile molecule.

Yield, 0.64 g (0.66 mmol, 70%). *Anal. Calc.* for $\text{C}_{41}\text{H}_{48}\text{F}_{12}\text{FeN}_8\text{P}_2$: C, 49.31; H, 4.84; N, 11.22. Found: C, 49.46; H, 4.85; N, 11.42%. In the ^1H NMR, 12 signals are expected for the complex, five are observed, the remaining signals are likely shifted and broadened into the baseline due to the paramagnetism of the compound. ^1H NMR (270 MHz, RT, DMSO- d_6): $\delta = 23.99$, 20.82, 12.88, 10.29, 4.50. Mößbauer parameters for $[(\text{TIMEN}^{3,5\text{xy}l})\text{Fe}](\text{PF}_6)_2$: $\delta = 0.52(1) \text{ mm s}^{-1}$, $\Delta E_Q = 1.12(1) \text{ mm s}^{-1}$, $\Gamma_{\text{FWHM}} = 0.50(1) \text{ mm s}^{-1}$. Mößbauer parameters for $[(\text{TIMEN}^{3,5\text{xy}l})\text{Fe}(\text{CH}_3\text{CN})](\text{PF}_6)_2$: $\delta = 0.73(1) \text{ mm s}^{-1}$, $\Delta E_Q = 1.08(1) \text{ mm s}^{-1}$, $\Gamma_{\text{FWHM}} = 0.36(1) \text{ mm s}^{-1}$.

2.4.8. $[(\text{TIMEN}^{3,5\text{xy}l})\text{Fe}]$ (**8**)

A solution of $[(\text{TIMEN}^{3,5\text{xy}l})\text{Fe}](\text{PF}_6)_2$ (0.30 g, 0.31 mmol) in THF was stirred overnight over an excess of sodium amalgam (5.60 g,

Na 0.8 wt.%). The solution was filtered through celite, concentrated *in vacuo* and cooled to -35°C to yield the product as dark red crystals.

Mößbauer parameters: $\delta = 0.14(1) \text{ mm s}^{-1}$, $\Delta E_Q = 2.29(2) \text{ mm s}^{-1}$, $\Gamma_{\text{FWHM}} = 0.93(3) \text{ mm s}^{-1}$.

2.4.9. $[(\text{TIMEN}^{3,5\text{xy}l})\text{Fe}](\text{PF}_6)$ (**9**)

Method A: $[(\text{TIMEN}^{3,5\text{xy}l})\text{Fe}]$ (200 mg, 0.30 mmol) was dissolved in 10 mL CHCl_3 to form a green solution. Excess of NaPF_6 was added and diethyl ether was then diffused into the filtered solution at room temperature to give green crystals overnight.

Method B: Addition of silver triflate (77 mg, 0.30 mmol) to a suspension of $[(\text{TIMEN}^{3,5\text{xy}l})\text{Fe}]$ (200 mg, 0.30 mmol) yielded a green solution and a dark grey precipitate of elemental silver. The solution was filtered through celite and the solvent was removed at reduced pressure to yield the green product.

EPR (acetonitrile, 86 K, 8.981690 GHz, ModWidth = 1.0 mT, Power = 1.00 mW) $g_1 = 2.42$, $g_2 = 2.20$, $g_3 = 1.94$.

2.5. Theoretical calculations

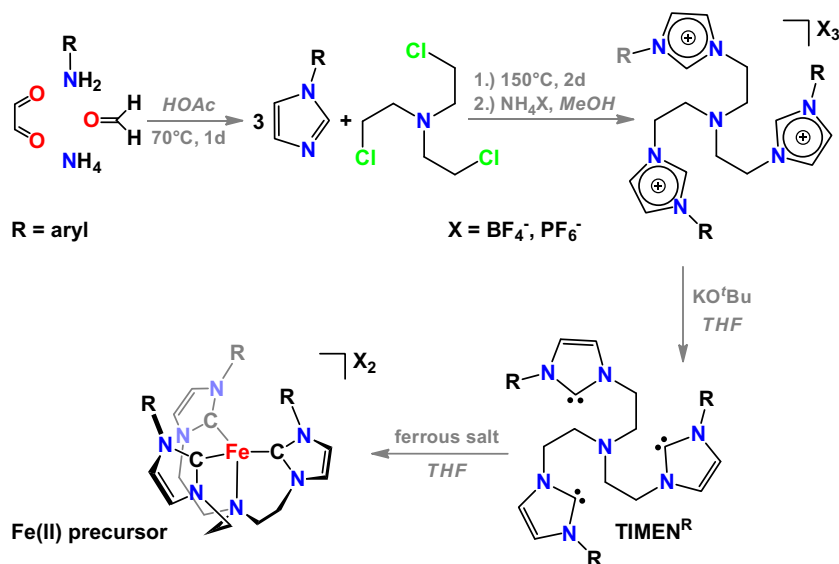
The program package ORCA 2.7 revision 0 was used for all calculations [16]. The geometry optimization calculations were performed by the spin-unrestricted DFT method with the BP86 [17–19] functional. The single point calculations and calculations of Mößbauer parameters were performed with the B3LYP functional [20–22]. The triple- ζ basis sets with one-set of polarization functions [23] (TZVP) were used for iron ions and the double- ζ basis sets with one-set of polarization functions [23] (SVP) were used for all other atoms. For calculation of Mößbauer parameters, the “core” CP(PPP) basis set for iron [24,25] was used. This basis is based on the TurboMole DZ basis, developed by Ahlrichs and co-workers and obtained from the basis set library under ftp.chemie.uni-karlsruhe.de/pub/basen. Molecular orbitals were visualized *via* the program MOLEKEL [26].

3. Results and discussion

The tripodal ligand system TIMEN^{R} (R = mesityl and 2,6-xylyl) has been successfully employed for the stabilization of metal centers in high and low oxidation states [9]. A general property of N-heterocyclic carbenes (NHCs) is the ability to act as both, a σ -donor, stabilizing high oxidation states, and as π -acceptor, providing the possibility for π -backbonding, thus also stabilizing low oxidation states at electron-rich metal ions. While for a long time NHCs were regarded as pure σ -donor ligands, it is now widely accepted that this class of ligand can also act as π -acceptor [2,3].

Recently, the synthesis of a discrete high-valent iron nitride complex was accomplished using a sterically encumbering N-anchored tris(carbene) ligand TIMEN^{R} , (R = aryl = 2,6-xylyl (xyl), mesityl (mes), Scheme 1) [9]. The reaction route toward these iron nitrides proceeds *via* deprotonation of the imidazolium salt $[\text{H}_3\text{TIMEN}^{\text{R}}]^{3+}$ with a base, like potassium *tert*-butoxide, yielding the N-heterocyclic carbene. Subsequent treatment of the free tripodal carbenes with FeCl_2 yields the four-coordinated Fe(II) complex $[(\text{TIMEN}^{\text{R}})\text{Fe}(\text{Cl})]\text{Cl}$, which can be reduced over sodium amalgam to afford the Fe(I) species $[(\text{TIMEN}^{\text{R}})\text{Fe}]\text{BPh}_4$. Addition of TMS-N_3 to the Fe(I) complex results in formation of Me_6Si_2 and the divalent complex $[(\text{TIMEN}^{\text{R}})\text{Fe}(\text{N}_3)]\text{BPh}_4$ which – after photolysis with UV light – yields the deeply purple colored Fe(IV) nitride complex $[(\text{TIMEN}^{\text{R}})\text{Fe}(\text{N})]\text{BPh}_4$. This N-anchored $\text{Fe}\equiv\text{N}$ complex is relatively unreactive and air- as well as moisture-stable in solid-state.

Interestingly, preliminary attempts to oxidize the Fe(IV) nitride complexes to Fe(V) species, unexpectedly lead to reduced bis-carbene imine species that formed *via* insertion of the terminal nitride



Scheme 1. Synthesis of TIMEN^R and the Fe(II) precursor complexes.

ligand into one of the iron – carbene bonds of the TIMEN^R ligand. This chemistry will be reported in due time and appears to be reminiscent to the insertion chemistry observed for the Co(III) imide complex, [(TIMEN^R)Co(NR)]BPh₄ [27]. The latter complex can be isolated at –35 °C but at room temperature forms similar bis-carbene imine species in solution.

Even in the presence of substrates, these examples of observed intramolecular insertion chemistry showed that the methyl groups in *ortho* position of the mesityl and 2,6-xylyl aryl rings of the NHC ligand play an important role in the reactivity of the corresponding iron complexes. Due to a strong steric shielding of the substituents on these positions, side-access of potential substrates to the axial M≡L functional group likely is efficiently suppressed, thereby preventing further reactivity of the Fe≡N unit in [(TIMEN^R)Fe(N)]BPh₄ and its oxidized Fe(V) species.

Aiming at high-valent metal complexes with axially bound terminal π-donor ligands, such as nitride, imides, and oxo ligands for atom and group transfer catalysis, we therefore synthesized two new tripodal carbene ligands with sterically less demanding aryl substituents, namely TIMEN^R (R = aryl = tolyl (tol), 3,5-xylyl (3,5xyl), Scheme 1). These ligands were employed in the synthesis of the corresponding Fe(II) precursor complexes in order to investigate their potential for the preparation of new low and high-valent iron complexes with enhanced reactivity.

Scheme 1 shows the general synthetic route to the tripodal ligand system. The first step is a one-pot reaction employing glyoxal, formaldehyde, ammonium salt, and an amine producing the derivatized imidazole [13]. The imidazoles can be linked to the framework anchor in an S_N²-type reaction with tris-(2-chloroethyl)amine [12]. Exchange of the Cl⁻ counterions to PF₆⁻ or BF₄⁻ anions leads to non-hygroscopic imidazolium salts [28]. Deprotonation of the imidazolium salt with a strong base, like potassium *tert*-butoxide, yields the N-heterocyclic carbene. Reaction of the free carbene with a ferrous salt like FeCl₂ or FeOTf₂ delivers the Fe(II) precursor complexes. The cationic Fe(II) precursor [(TIMEN^{tol})Fe]²⁺ was obtained *via* convenient one-pot synthesis, a new and viable alternative route for the synthesis of Fe(II) precursors of the TIMEN system. In this one-pot synthesis, a mixture of [H₃TIMEN^R](BF₄)₃, NaO^tBu, NaBPh₄, and FeCl₂ in THF is stirred overnight, followed by recrystallization of the crude product.

The [(TIMEN^{tol})Fe](BF₄)₂ complex exhibits a Mössbauer isomer shift, δ , of 0.51(1) mm s⁻¹ ($\Delta E_Q = 1.54(1)$ mm s⁻¹), slightly smaller

than typically observed for four-coordinate Fe(II) high-spin complexes of this system ($\delta \approx 0.65$ – 0.75 mm s⁻¹) [9].

The molecular structure of the cation [(TIMEN^{tol})Fe]²⁺ (Fig. 1) in crystals of [(TIMEN^{tol})Fe](BF₄)₂·0.8Et₂O (3·0.8Et₂O), obtained from a solvent mixture of acetonitrile and diethyl ether, exhibits a four-coordinated iron center with three equivalent iron carbene distances (average Fe–C_{carbene} distance 2.051 Å) and an Fe–N_{anchor} distance of 2.204(2) Å, clearly indicating a coordinated N-anchor.

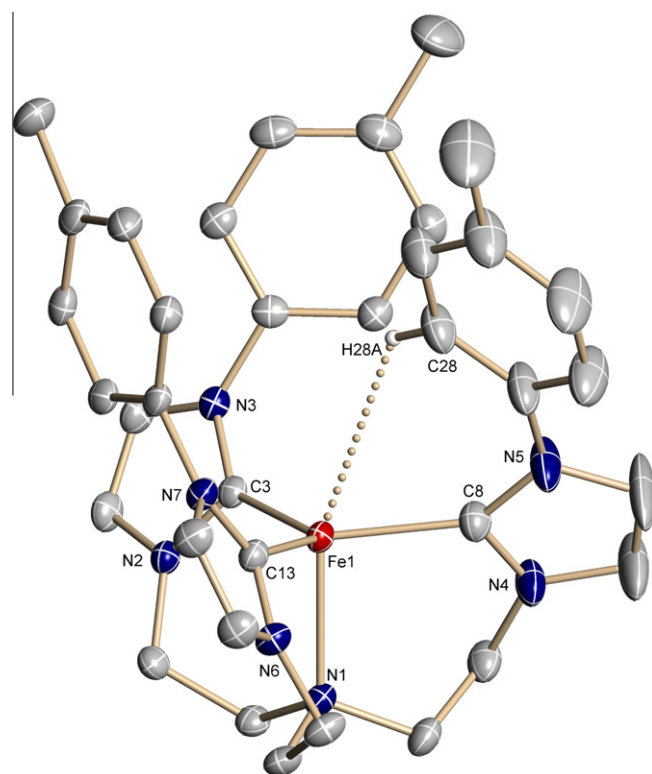
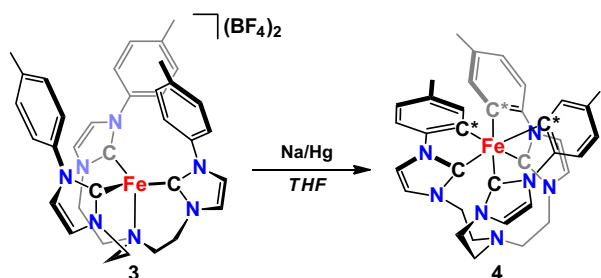


Fig. 1. Molecular structure of the complex cation of [(TIMEN^{tol})Fe](BF₄)₂ (3) in crystals of 3·0.8Et₂O (50% probability ellipsoids). Hydrogen atoms (except H28A), BF₄⁻ anions, and co-crystallized solvents are omitted for clarity. The dotted line indicates the weak anagostic Fe···H interaction.

The metal center is located 0.197(2) Å below the trigonal plane of the three NHC carbene carbon atoms. It is remarkable that, although present in the reaction mixture, no axially bound ligand, like chloride or acetonitrile, is observed in the crystallographically determined structure of **3**. This is in contrast to the Fe(II) complexes of the related TIMEN^{mes} and TIMEN^{xy} system with deep cylindrical cavities formed by the aryl substituents. For these complexes, axial coordination is always observed in the presence of coordinating anions or solvents. A possible reason for this could be the lack of methyl groups in 2- and 6-position of the aryl substituents in complexes of [(TIMEN^{tol})Fe]²⁺, allowing free rotation of the tolyl arms of the ligand, and thereby, preventing the formation of an accessible ligand cavity for axial coordination in the TIMEN^{tol} system. This rotational freedom is efficiently suppressed in ligands of the mesityl and 2,6-xylyl ligand derivatives. Furthermore, a close inspection of the structurally determined tolyl hydrogen atoms reveals that at least one of the *ortho* aryl C–H hydrogen atoms is pointing towards the center of the cavity and is thereby additionally blocking ligand access. The Fe1···H28A distance of



Scheme 2. Cyclometallation of [(TIMEN^{tol})Fe]²⁺ under reductive conditions.

2.90 Å and the corresponding Fe1···H28A–C28 angle of 122° is indicative for a weak and largely electrostatic interaction (anagostic interaction) [29].

Attempts to reduce the Fe(II) ion in complex **3** with sodium amalgam yield a different product than observed for the mesityl and 2,6-xylyl derivatives (Scheme 2). Instead of the expected formation of the reduced Fe(I) species, the oxidized, threefold cyclo-metallated σ -aryl Fe(III) complex [(TIMEN^{tol*})Fe] (**4**) was isolated (Fig. 2).

The EPR spectrum of a frozen solution of **4** shows an axial-symmetrical signal with resonances centered at $g_{\parallel} = 2.29$ and $g_{\perp} = 1.94$. This is in agreement with the complexes' axially distorted octahedral symmetry and a ground state of $S = 1/2$. As expected for a low-spin Fe(III) complex, the Mößbauer isomer shift of $\delta = 0.03(1) \text{ mm s}^{-1}$ ($\Delta E_Q = 2.37(1) \text{ mm s}^{-1}$) is considerably smaller than that of the Fe(II) precursor complex **3** (0.51 mm s^{-1}) and larger than that of the Fe(IV) nitride species (d^4 , low-spin, $S = 0$, $\delta = -0.27 \text{ mm s}^{-1}$). This confirms, that, despite the different coordination geometries and spin states of the complexes, the trend of decreasing isomer shifts with increasing oxidation states in ⁵⁷Fe Mößbauer spectroscopy is confirmed within this series of complexes.

The pseudo-octahedral Fe center of [(TIMEN^{tol*})Fe] (**4**) in crystals of **4**·2THF coordinates three NHC donors and three σ -aryl carbanions (denoted with an asterisk* in Scheme 2) with a *facial* arrangement of each of the two different sets of C donor atoms. In this complex, the iron center is coordinated by three bidentate ligand arms with every NHC carbon situated *trans* to a C* carbon atom of an aryl ring. It is remarkable, however, that in **4** one of the Fe–C* bonds, Fe–C24 = 2.366(2) Å, is significantly longer, by ~0.35 Å, than the other two Fe–C_{carbene} bonds. The shortest bond (Fe–C3 = 1.888(2) Å) is *trans* to this longest bond (Table 3). In contrast, a perfectly symmetrical arrangement is observed for *fac*-[Ir{CN(C₆H₄Me-*p*)(CH₂)₂NC₆H₃Me-*p*)₃] [30], a homoleptic complex exhibiting exactly the same coordination mode with three NHC donors (Ir–C_{avg} 2.03(3) Å) and three *trans* coordinated aryl carbanions (Ir–C_{avg} 2.09(3) Å). It is reasonable to assume that the three individual bidentate ligands, coordinating the iridium in

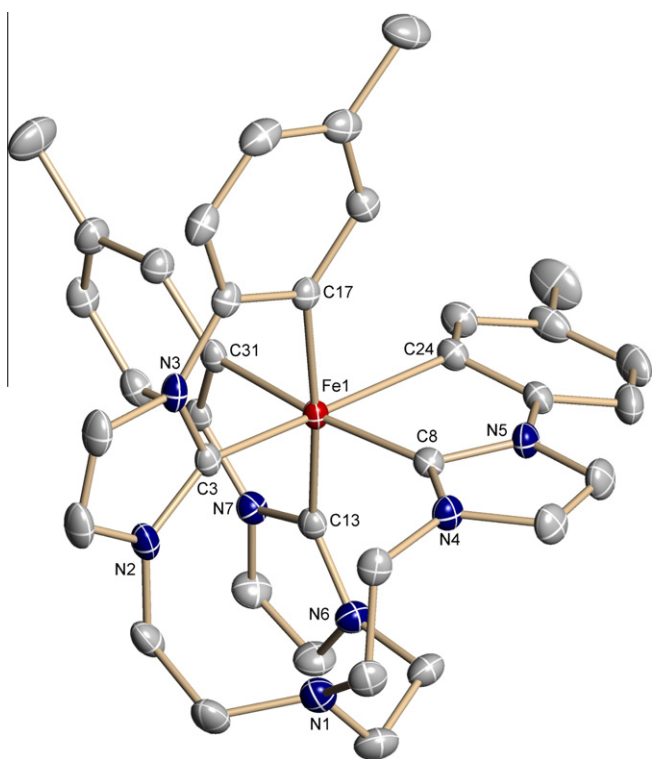


Fig. 2. Molecular structure of [(TIMEN^{tol*})Fe] in crystals of **4**·2THF (50% probability ellipsoids). Hydrogen atoms and co-crystallized solvents omitted for clarity.

Table 3
Selected bond distances (Å) and angles (°) for molecular structures of **3**, **4**, **7**, **8** and **9** (e.s.d's in parentheses).

Compounds	3	4	7	8	9
Fe–C3	2.046(2)	1.888(2)	2.101(3)	1.913(2)	1.972(3)
Fe–C8	2.055(2)	1.923(2)	2.108(3)	1.870(2)	1.895(3)
Fe–C13	2.052(2)	1.943(2)	2.107(3)	1.941(2)	1.999(3)
Fe–N1	2.204(2)	3.947(2)	2.545(3)	3.936(2)	3.935(3)
Fe–N8	–	–	2.193(2)	–	–
Fe–C17	–	1.994(2)	–	2.442(2)	2.525(3)
Fe–C24 ^{#1}	–	2.366(2)	–	2.050(2)	2.032(3)
Fe–C31 ^{#2}	–	2.014(2)	–	2.074(2)	2.037(3)
C3–Fe–C8	121.73(9)	100.01(8)	117.9(2)	101.10(8)	103.4(2)
C3–Fe–C13	118.81(8)	97.59(9)	120.1(2)	93.73(8)	91.3(2)
C8–Fe–C13	116.73(9)	97.46(9)	120.2(2)	95.53(8)	93.9(2)
C3–Fe–N1	96.67(8)	–	85.0(1)	–	–
C8–Fe–N1	95.34(8)	–	85.6(1)	–	–
C13–Fe–N1	94.45(8)	–	86.0(1)	–	–
C3–Fe–C17	–	82.12(9)	–	78.52(8)	–
C8–Fe–C17	–	89.77(8)	–	176.17(7)	–
C13–Fe–C17	–	172.69(8)	–	80.71(8)	–
C3–Fe–C24 ^{#1}	–	178.01(8)	–	87.40(8)	86.6(2)
C8–Fe–C24 ^{#1}	–	78.86(8)	–	82.53(8)	82.1(2)
C13–Fe–C24 ^{#1}	–	84.20(8)	–	177.92(8)	174.9(2)
C3–Fe–C31 ^{#2}	–	89.12(8)	–	169.64(8)	169.1(2)
C8–Fe–C31 ^{#2}	–	170.87(8)	–	88.44(8)	85.9(2)
C13–Fe–C31 ^{#2}	–	91.69(8)	–	81.22(8)	82.2(2)

^{#1} C24 corresponds to C25 in complexes **8** and **9**.

^{#2} C31 corresponds to C33 in complexes **8** and **9**.

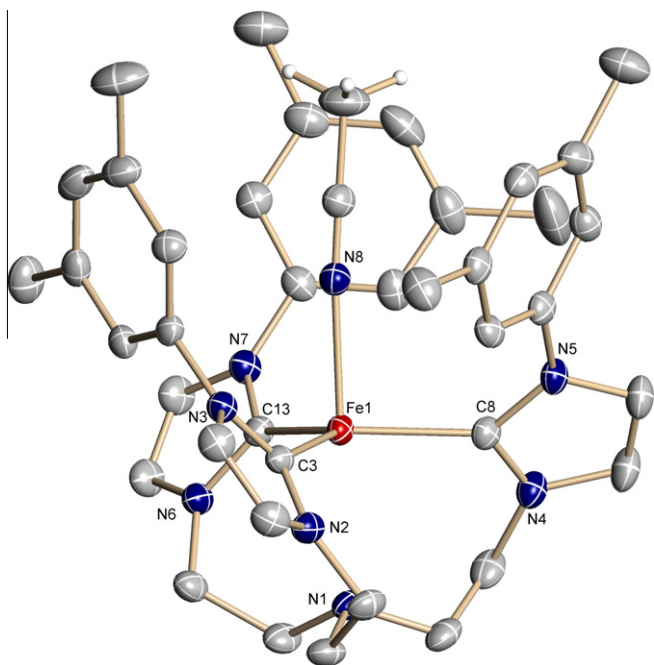


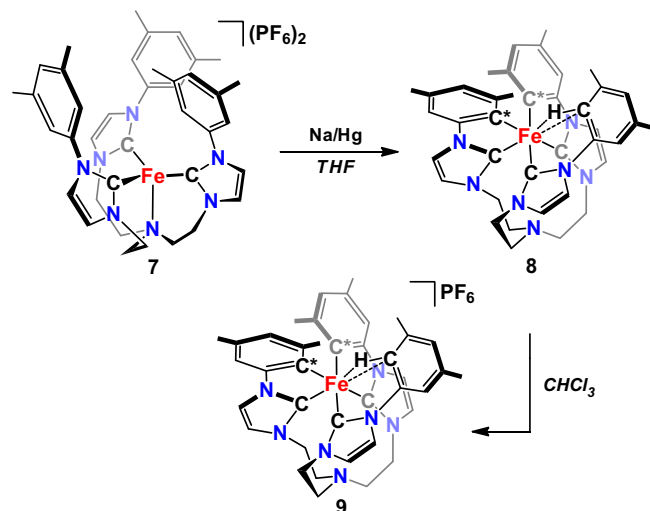
Fig. 3. Molecular structure of the complex cation of $[(\text{TIMEN}^{3,5\text{-xyly}})\text{Fe}(\text{CH}_3\text{CN})](\text{PF}_6)_2$ (**7**) in crystals of $7 \cdot 2\text{CH}_3\text{CN}$ (50% probability ellipsoids). Hydrogen atoms of the $\text{TIMEN}^{3,5\text{-xyly}}$ ligand, the PF_6^- anions, and co-crystallized solvents are omitted for clarity.

$\text{fac-}[\text{Ir}(\text{CN}(\text{C}_6\text{H}_4\text{Me-}p)(\text{CH}_2)_2\text{NC}_6\text{H}_3\text{Me-}p)_3]$, are free to arrange in a symmetrical fashion around the metal center, while the flexibility of the tripodal TIMEN^R ligand with three N-tethered carbene aryl entities is reduced, resulting in the observed non-symmetrical binding mode to the smaller iron ion. This may also result in ligand distortions. For instance, two of the ligand arms in **4**, the five-membered NHC ring and the adjacent aryl ring, are almost coplanar, whereas the two rings of the third ligand arm with a considerably longer $\text{Fe}-\text{C}^*$ bond exhibit a significant deviation from coplanarity. The torsion angles $\text{C}^*-\text{C}_{\text{aryl}}-\text{N}-\text{C}_{\text{carbene}}$ are a good measure of the coplanarity of the five-membered imidazol-2-ylidene and aryl ring systems and amount to only $0.6(2)^\circ$ for $\text{C}3-\text{N}3-\text{C}16-\text{C}17$ and $2.4(3)^\circ$ for $\text{C}13-\text{N}7-\text{C}30-\text{C}31$, but to $17.1(3)^\circ$ for $\text{C}8-\text{N}5-\text{C}23-\text{C}24$.

In an effort to suppress the observed intramolecular metallacycle formation, an alternative approach was sought off. The introduction of 3,5-xylyl substituents into the TIMEN -ligand system (instead of mesityl and 2,6-xylyl groups) is expected to slightly increase the distance of the *ortho* C–H groups from the Fe center. This should effectively prevent metallation of the reactive *ortho* C–H bonds, and thus, provide a chelating ligand with increased side-access to the $\text{M}=\text{E}$ functional group.

Treatment of the free 3,5-xylyl derivatized tris(carbene) with ferrous chloride in a mixture of THF and pyridine, followed by recrystallization from acetonitrile, yields the corresponding Fe(II) precursor complex $[(\text{TIMEN}^{3,5\text{-xyly}})\text{Fe}(\text{CH}_3\text{CN})](\text{PF}_6)_2$ (**7**) (Fig. 3). Complex **7** exhibits a Mössbauer isomer shift of $\delta = 0.73(1) \text{ mm s}^{-1}$ ($\Delta E_Q = 1.08(1) \text{ mm s}^{-1}$), characteristic of a four-coordinate Fe(II) high-spin ($S = 2$) species of this system.

In contrast to $[(\text{TIMEN}^{\text{tol}})\text{Fe}]^{2+}$ (**3**) with rotatable tolyl substituents, rotation of the aryl substituents in **7** is hindered by the methyl groups in 3,5-position. Therefore, the steric demand of the 3,5-substituted aryl arm in **7** is expectedly higher and results in an axial cavity large enough to accommodate an axially bound acetonitrile ligand. The Fe(II) center in crystals of $[(\text{TIMEN}^{3,5\text{-xyly}})\text{Fe}(\text{CH}_3\text{CN})](\text{PF}_6)_2 \cdot 2\text{CH}_3\text{CN}$ is coordinated in a trigonal pyramidal fashion with three equivalent $\text{Fe}-\text{NHC}$ carbon bonds, with an



Scheme 3. Cyclometallation of $[(\text{TIMEN}^{3,5\text{-xyly}})\text{Fe}]^{2+}$ under reductive conditions.

average $\text{Fe}-\text{C}_{\text{carbene}}$ distance of 2.105 \AA , and a coordinated acetonitrile ligand ($\text{Fe}-\text{N}_{\text{CH}_3\text{CN}}$ distance of $2.193(2) \text{ \AA}$). The iron center is situated $0.164(2) \text{ \AA}$ above the trigonal plane formed by the three NHC carbene donor atoms. Due to the axial coordination of an acetonitrile molecule, the $\text{Fe}-\text{N}_{\text{anchor}}$ distance of $2.545(3) \text{ \AA}$ is considerably longer than that found in $[(\text{TIMEN}^{\text{tol}})\text{Fe}]^{2+}$ and shows that the N-anchor is no longer coordinated in **7**.

The ability of the $[(\text{TIMEN}^{3,5\text{-xyly}})\text{Fe}]^{2+}$ moiety to accommodate an axial ligand (as was observed earlier for the corresponding mesityl and 2,6-xylyl derivatives) prompted us to attempt the synthesis of a high-valent iron nitride complex. In order to synthesize the required Fe(I) precursor complexes $[(\text{TIMEN}^R)\text{Fe}]^+$, reduction of **7** using the sodium amalgam protocol used for the reduction of $[(\text{TIMEN}^{\text{mes/xyly}})\text{Fe}(\text{Cl})]^+$ was performed. However, different from the complexes of the mesityl- and 2,6-xylyl ligand derivatives, and reminiscent to the observations made for the tolyl derivative **3** (*vide supra*), the reduction of the Fe(II) complex **7** yielded yet another Fe(II) metallation product (Scheme 3).

The Mössbauer spectrum of a solid sample of this Fe(II) complex shows a doublet with an isomer shift of $0.14(1) \text{ mm s}^{-1}$ and a quadrupole splitting, ΔE_Q , of $2.29(2) \text{ mm s}^{-1}$. These Mössbauer parameters are remarkably different from its Fe(II) precursor ($\delta = 0.73(1) \text{ mm s}^{-1}$ ($\Delta E_Q = 1.08(1) \text{ mm s}^{-1}$), and are indicative of an Fe(II) low-spin ($S = 0$) species in an octahedral ligand environment, as opposed to the four-coordinate Fe(II) high-spin ($S = 2$) precursor. However, the metallated Fe(II) complex does not give ^1H NMR spectra, suggesting that this complex is high-spin, $S = 2$, in solution.

The results of an X-ray crystal structure determination confirmed the formation of a pseudo-octahedrally coordinated bis-metallated Fe(II) complex, namely $[(\text{TIMEN}^{3,5\text{-xyly}^*})\text{Fe}]$ (**8**) (Fig. 4), rather than the tris-metallated Fe(III) species **4**.

The pseudo-octahedral iron center in **8** coordinates to three facially arranged N-heterocyclic carbene donors and two σ -aryl carbonions (denoted with an asterisk * in Scheme 3). The Fe ion's distorted octahedral coordination environment is completed with an agostic hydrogen interaction to one of the aryl's *ortho* CH groups, namely H17A. The position of the hydrogen atom of this non-dehydrogenated aryl CH group could be experimentally determined from the difference Fourier map. However, for reasons of consistency, H17A was placed in an idealized position of optimized geometry during refinement.

The $\text{Fe}-\text{C}$ bond distances in **8** are similar to those observed in **4** and the shorter NHC–Fe bond distances are compensated by longer

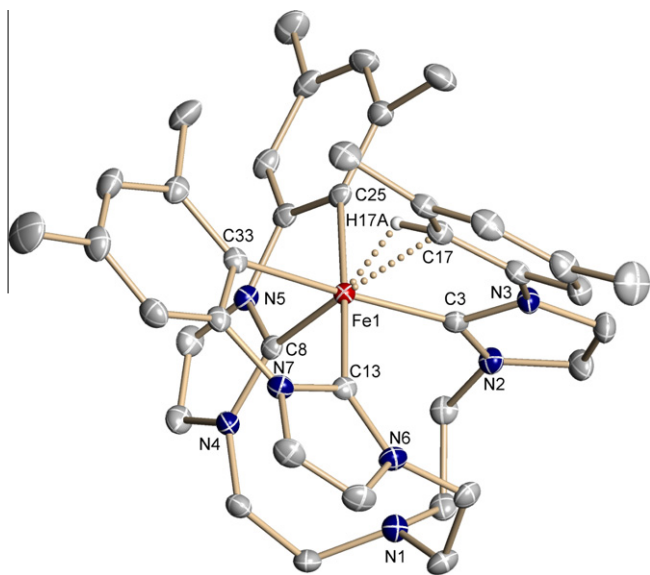


Fig. 4. Molecular structure of $[(\text{TIMEN}^{3,5\text{-xylyl}})^+\text{Fe}]$ (**8**) (50% probability ellipsoids). Hydrogen atoms (except H17A) omitted for clarity. Dotted lines indicate the agostic $\text{Fe}\cdots\text{H}$ interaction.

$\text{Fe}-\text{C}^*$ carbanion distances. The shortest iron carbene distance of 1.870(2) Å for Fe–C8 is observed *trans* to the CH of the non-dehydrogenated ring ($\text{Fe}\cdots\text{C17} = 2.442(2)$ Å and $\text{Fe}\cdots\text{H17A} = 1.71$ Å, $\text{Fe1}\cdots\text{H17A}-\text{C17} = 131^\circ$), which also exhibits the strongest deviation from co-planarity of the NHC and the 3,5-xylyl rings. When comparing the distortion between the NHC and aryl moieties in both, the tolyl and the 3,5-xylyl derivatives, it is obvious that the 3,5-substitution of the aryl ring is increasing the steric demand. As observed in the molecular structure of **4**, two of the NHC–aryl systems of **8** are almost perfectly coplanar with corresponding torsion angles of $4.3(2)^\circ$ for C8–N5–C24–C25 and $1.7(2)^\circ$ for C13–N7–C32–C33. The N-heterocyclic carbene and 3,5-xylyl moieties of the third pendant ligand arm, however, are significantly tilted, reflected by the C3–N3–C16–C17 torsion angle of $27.4(3)^\circ$ (as compared to $17.1(3)^\circ$ found in the sterically less crowded tolyl derivative **4**).

The bis-metallated complex $[(\text{TIMEN}^{3,5\text{-xylyl}})^+\text{Fe}]$ (**8**) can be easily oxidized to yield a green colored Fe(III) complex (Scheme 3). This oxidation occurs readily and even during simple work-up of **8** in halogenated solvents. A straightforward synthesis was accomplished by treatment of **8** with silver salts, like AgOTf, in acetonitrile. The molecular structure of the resulting complex $[(\text{TIMEN}^{3,5\text{-xylyl}})^+\text{Fe}](\text{PF}_6)$ (**9**) is depicted in Fig. 5.

In analogy to **4**, the EPR spectrum of a frozen acetonitrile solution of **9**, with *g*-values of $g_1 = 2.42$, $g_2 = 2.20$, $g_3 = 1.94$, confirms the $S = 1/2$ ground state of this low-spin Fe(III) complex.

In **9**, the Fe(III) center is pseudo-octahedrally coordinated and all metric parameters of the molecular structure are very similar to those observed for the Fe(II) complex **8**. Slight differences are observed only for the Fe–C distances with longer iron carbene bonds and shorter iron carbanion bonds compared to those found in the Fe(II) species (Table 3). Compared to **8**, the Fe(III)– CH_{aryl} bond distance in **9** is slightly longer and was determined to be $\text{Fe}\cdots\text{C17} = 2.525(3)$ Å. The other relevant distances are $\text{Fe}\cdots\text{H17A} = 1.79$ Å and $\text{Fe1}\cdots\text{H17A}-\text{C17} = 131^\circ$ and are again representing an agostic interaction. This elongation of bond distances in **9** is most likely due to the smaller ionic radius of the Fe(III) ion, compared to the divalent Fe center in **8**. The third arm of the ligand shows a significant tilt between the NHC and the 3,5-xylyl moiety evidenced by the C3–N3–C16–C17 torsion angle of $25.7(4)^\circ$. The

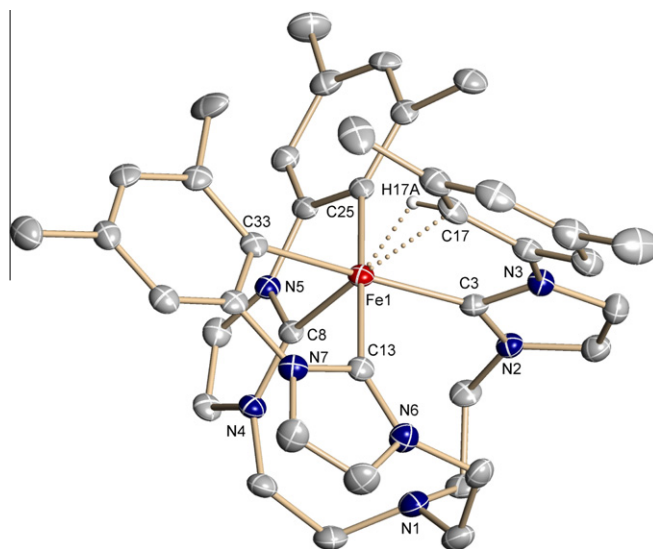


Fig. 5. Molecular structure of the complex cation of $[(\text{TIMEN}^{3,5\text{-xylyl}})^+\text{Fe}]$ in crystals of **9**:0.6THF:0.4CHCl₃ (50% probability ellipsoids). Hydrogen atoms (except H17A), PF_6^- anion, and co-crystallized solvents are omitted for clarity. The dotted lines indicate the agostic $\text{Fe}\cdots\text{H}$ interaction.

other two NHC carbene aryl moieties remain coplanar (the corresponding torsion angles C8–N5–C24–C25 and C13–N7–C32–C33 amount to $0.1(4)^\circ$ and $0.4(4)^\circ$, respectively).

In general, the overall coordination environment with two almost ideally coplanar arranged aryl–carbene moieties, short iron NHC distances, and one elongated iron CH_{aryl} distance, corresponding to the tilted ligand arm *trans* to the shortest Fe – NHC bond, does not change between the bis-metallated Fe(II) and Fe(III) centers in complexes **8** and **9**.

4. Theoretical considerations

The electronic structures of **4**, **8**, and **9** were additionally examined by density functional theory (DFT) calculations. The geometries of the complexes have been fully optimized by using the BP86 functional (Table 4). The optimized structures of **8** and **9** are in excellent agreement with the available X-ray structures showing the presence of agostic $\text{Fe}\cdots\text{H}$ interactions (Table 4). In contrast, the experimental structure of **4** possesses an axially distorted octahedral geometry, whereas the calculated structure is symmetrical, showing a set of three similar Fe–C* and a set of three similar Fe–C_{NHC} bonds.

Attempts to optimize the molecular structure of **4** by using larger basis sets, by including relativistic effects, a conductor like screening model (COSMO), and by including empirical van der

Table 4

Principal bond distances of the optimized structures as obtained from the spin-unrestricted BP-DFT calculations.

	4	8	9
Fe–C _{NHC}	1.964 (1.943) ^a	1.897 (1.913)	2.011 (1.990)
Fe–C ^b	2.016 (1.994)	2.092 (2.074)	2.041 (2.032)
Fe–C _{NHC}	1.962 (1.923)	1.940 (1.940)	1.983 (1.972)
Fe–C	2.014 (2.014)	2.074 (2.050)	2.055 (2.037)
Fe–C _{NHC}	1.962 (1.888)	1.872 (1.870)	1.882 (1.895)
Fe–C	2.015 (2.366)	2.468 (2.442)	2.593 (2.524)
Fe $\cdots\text{H}^c$	–	1.782 (1.708)	1.883 (1.795)

^a The experimental values are given in parentheses.

^b *trans* to C_{NHC}.

^c Agostic interactions.

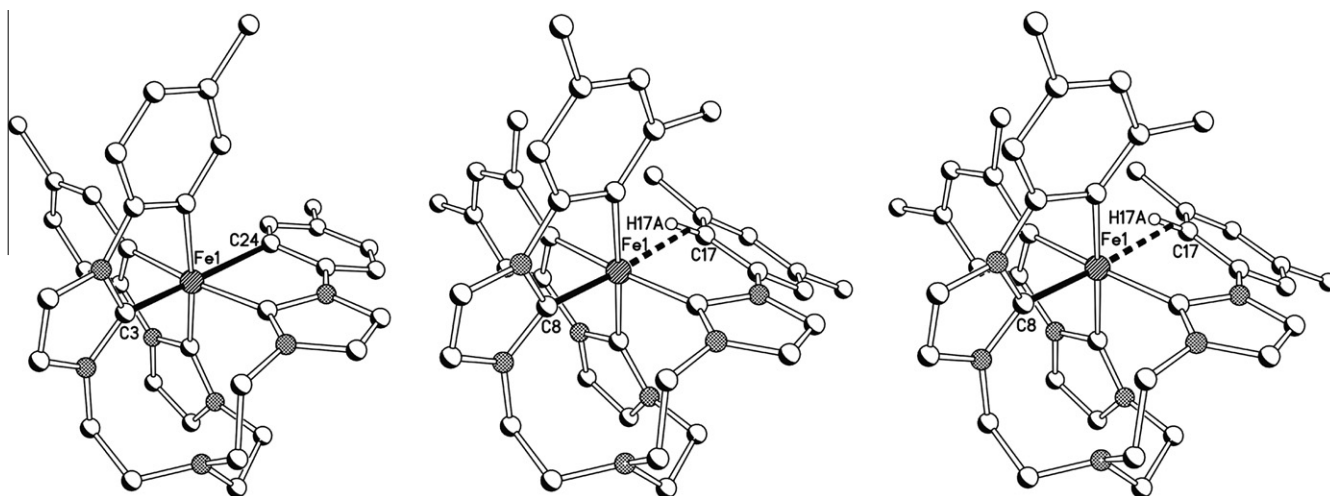


Fig. 6. Molecular representations of complexes **4** (left), **8** (middle), and cation **9** (right), the axial distortion highlighted in bold.

Waals corrections all gave very similar, symmetrical structures. Therefore, based on the DFT calculations, it appears that – in principle – the ligand is sufficiently flexible to coordinate the Fe ion in a symmetrical fashion with three facially coordinating NHC carbon and three metallated aryl carbon ligands. It is, however, quite remarkable that the tris-metallated Fe(III) complex **4** and the bis-metallated Fe(II) and Fe(III) complexes **8** and **9** show a similar departure from octahedral symmetry with an axial distortion (one short Fe – C_{NHC} and one long Fe–C_{aryl} bond and agostic Fe··CH interaction *trans* to it, respectively, see Fig. 6 and Table 5).

It can be speculated that the observed structural distortion in **4** originates from electronic (Jahn–Teller distortion), steric (ligand flexibility) or even crystal packing effects. The phenomenon appears too pronounced, however, to be entirely due to crystal packing effects. It also seems unlikely that such a packing effect can be observed in three different crystal structures. Alternatively, one could also argue that d^5 low-spin complexes ($S = 1/2$), such as **4** and **9**, are subject to a Jahn–Teller distortion, and hence, the observed structural distortion could be the result of the Jahn–Teller effect, leading to a non-degenerate ground state. However, complex **8** is a low-spin Fe(II) complex ($S = 0$), for which no Jahn–Teller

effect is expected. On the other hand, while there is no apparent steric hindrance in **4**, it appears reasonable to assume that steric pressure, exerted by the aryl methyl groups in the 3,5-xylyl-derivatized species, effectively prevents tris-metallation in complex **8**, which results in one weak Fe··CH agostic interaction and one short Fe–C_{NHC} bond of 1.870 Å *trans* to it. This may also explain the observed torsion angles within the five-membered NHC and the aryl substituent, which are more pronounced in the [(TIME-

Table 5

Principal bond distances of the observed structures as obtained from the X-ray crystal structure determination

	4	8	9
Fe–C _{NHC}	1.943 ^a	1.913	1.999
Fe–C	1.994	2.074	2.032
Fe–C _{NHC}	1.923	1.941	1.972
Fe–C	2.014	2.050	2.037
Fe–C _{NHC}	1.888	1.870	1.895
Fe–C	2.366	–	–
Fe··CH ^a	–	2.053	2.138

^a These values refer to the distance between Fe and the middle of the CH bond.

Table 6

Mössbauer parameters of **4**, **8**, and **9** obtained from the spin-unrestricted B3LYP-DFT calculations.

	4	8	9
δ (mm s ⁻¹)	-0.11 (+0.03) ^a	+0.05 (+0.11)	-0.01 ^b
ΔE_Q (mm s ⁻¹)	+2.12 (2.37)	+2.34 (2.29)	1.30 ^b

^a The experimental values are given in parentheses.

^b No experimental data available.

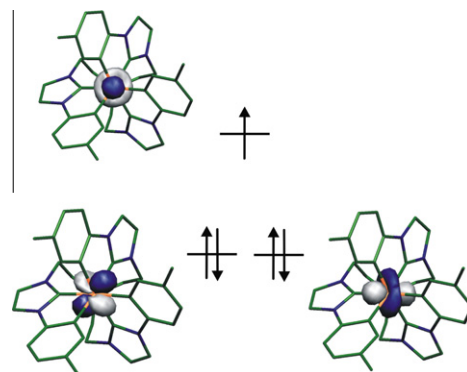


Fig. 7. Occupied frontier iron-based MOs for **4** as obtained from the spin-unrestricted B3LYP-DFT calculations: quasi-restricted orbitals are shown, all three MOs are mixtures of d_{xy} , d_{xz} , and d_{yz} iron orbitals.

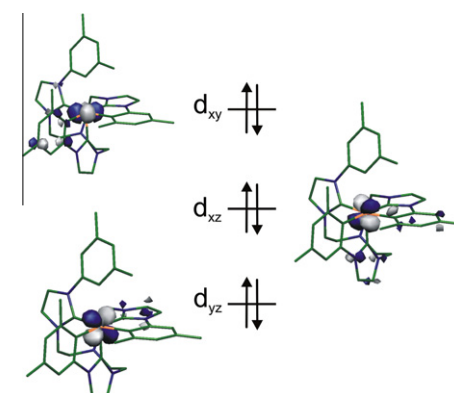


Fig. 8. Occupied frontier iron-based MOs for **8** as obtained from the spin-unrestricted B3LYP-DFT calculations: canonical orbitals are shown.

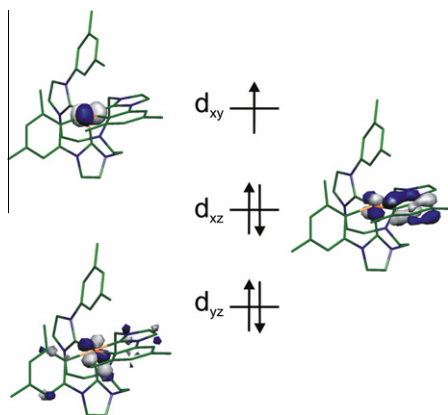


Fig. 9. Occupied frontier iron-based MOs for **9** as obtained from the spin-unrestricted B3LYP-DFT calculations: quasi-restricted orbitals are shown.

$N^{3,5\text{-xyl}^{1**}}\text{Fe}]^{0/+}$ complexes **8** and **9** compared to the tolyl-derivatized species **4**.

In summary, whereas the axially distorted, pseudo-octahedral structures of **8** and **9** can be theoretically reproduced and explained on the basis of steric pressure, the reason for the axial distortion in **4** and its discrepancy to the computationally calculated structure remains unclear.

The Mößbauer parameters for **4**, **8**, and **9** were also calculated at the B3LYP level of DFT (Table 6). Interestingly, and despite the failure to reproduce the experimentally determined structure of **4**, all calculated parameters reproduce the experimentally determined values accurately. The calculated complexes exhibit isomer shifts typical for low-spin ferrous and low-spin ferric ions.

The calculated electronic structures confirm the presence of a low-spin ferrous ion in **8** and a low-spin ferric ion in **4** and **9**. Several attempts to calculate intermediate- and high-spin species resulted in significant discrepancy between the calculated and the experimental molecular structures. This further confirms the low-spin ground states for **4**, **8**, and **9**. All doubly and singly occupied molecular orbitals (MOs) with significant iron d-character were identified among the sets of canonical or quasi-restricted MOs (Figs. 7–9). The unoccupied d-orbitals are highly delocalized and are not shown. The approximate C_3 symmetry of the complex **4** results in strong mixing of d-orbitals within the t_{2g} set. However, d-orbital mixing in **8** and **9** is lower than in **4** due to the less symmetrical molecular structures of **8** and **9**. Hence, the one-electron oxidation **8** → **9** can computationally be shown to result in the loss of one-electron from mainly the d_{xy} metal orbital.

5. Conclusion

The reduced reactivity of the first generation complexes [(TIMEN^R)Fe] was attributed to the steric demand exerted by the mesityl and 2,6-xylyl substituents. In an effort to enhance the reactivity of the various low- and high-valent iron complexes of the TIMEN^R ligand system (R = aryl = mesityl (mes), 2,6-xylyl (xyl)), two new ligands and their corresponding iron complexes were synthesized and spectroscopically characterized. Throughout the syntheses of the iron complexes, unexpected reactivities were observed with these new ligand systems, resulting in a series of new four, five, and six-coordinate complexes. The divalent iron precursor complexes **3** and **7**, tris-metallated **4**, and the bis-metallated complexes **8** and **9**, as well as the imidazolium salts of the ligands (see deposited data) were characterized by single crystal X-ray structure determination and spectroscopic methods.

As predicted, introduction of sterically less demanding aryl substituents bearing potential reactive C–H bonds in *ortho* position of the aromatic rings changes the reactivity of the Fe(II) precursor complexes. Introduction of the tolyl group reduced the steric pressure in a way that the aryl groups are now free to rotate thereby preventing coordination of an axial ligand in the corresponding Fe(II) complex **3**. In contrast, replacing the tolyl with 3,5-xylyl groups resulted in the formation of an Fe(II) precursor complex **7** with an accessible axial coordination cavity. From the structure determinations of the Fe(II) precursor complexes **3** and **7** it is evident that the steric demand is significantly reduced. However, these Fe(II) precursor complexes exhibit unpredicted reactivities that differ significantly from the mesityl and 2,6-xylyl derivatives. Attempts to reduce the Fe(II) precursors over sodium amalgam did not yield the expected Fe(I) complexes. Instead, cyclometallation of the aryl carbene moieties leading to pseudo-octahedrally coordinated, tris-metallated (in the case of the tolyl system) or bis-metallated (for the 3,5-xylyl system) Fe(II) and Fe(III) complexes. While the tris-metallated species [(TIMEN^{tol})Fe] (**4**) is relatively stable towards oxidation, the bis-metallated [(TIMEN^{3,5xyl})Fe] (**8**) is easily oxidized to yield the corresponding Fe(III) compound [(TIMEN^{3,5xyl})Fe](PF₆) (**9**). The observed structural parameters demonstrate that this ligand framework is well suited to coordinate iron centers in a trigonal pyramidal fashion with three equivalent ligand arms. An octahedral coordination of the central metal requires a twist of the third ligand arm that features large twist angles between the five-membered NHC ring and the adjacent aryl ring of 17.1(3)° (for **4**), 27.4(3)° (for **8**) and of 25.7(4)° (for **9**). Reducing the steric demand of the TIMEN^R ligand system by introducing aryl rings with no substituents in the 2,6-position was successfully achieved. However, the two new ligands TIMEN^{tol} and TIMEN^{3,5xyl} yielded Fe(II) precursor complexes **3** and **7** that again showed unexpected reactivities upon reduction, very different than observed for the mesityl and 2,6-xylyl derivatives. Obviously, relatively small changes in the periphery of the ligand have drastic effects on the reactivity of the resulting complexes. Future work will aim at fine-tuning the TIMEN^R ligand system even further by introducing other aryl substituents for the synthesis of Fe≡N complexes with enhanced reactivity.

Appendix A. Supplementary material

CCDC 776777, 776778, 776779, 776780, 776781, 776782 and 776783 contain the supplementary crystallographic data for **1**(CF₃SO₃)₃, [H₃TIMEN^{tol}](CF₃SO₃)₃, **3** · 0.8 Et₂O, [(TIMEN^{tol})Fe]-(BF₄)₂ · 0.8 Et₂O, **4** · 2 THF, [(TIMEN^{tol})Fe] · 2 THF, **5**(Cl)₃ · solv, [H₃TIMEN^{3,5xyl}](Cl)₃ · solv, **7** · 2 CH₃CN, [(TIMEN^{3,5xyl})Fe(CH₃CN)]-(PF₆)₂ · 2 CH₃CN, **8**, [(TIMEN^{3,5xyl})Fe] and **9** · 0.6 THF · 0.4 CHCl₃, [(TIMEN^{3,5xyl})Fe](PF₆) · 0.6 THF · 0.4 CHCl₃. These data can be obtained free of charge from The Cambridge Crystallographic Data Centre via www.ccdc.cam.ac.uk/data_request/cif.

Supplementary data associated with this article can be found, in the online version, at [doi:10.1016/j.ica.2010.07.039](https://doi.org/10.1016/j.ica.2010.07.039).

References

- [1] W.B. Tolman (Ed.), Activation of Small Molecules: Organometallic and Bioinorganic Perspectives, Wiley-VCH, Weinheim, 2006.
- [2] M. Alcarazo, T. Stork, A. Anoop, W. Thiel, A. Fürstner, *Angew. Chem., Int. Ed.* **49** (2010) 2542.
- [3] X. Hu, Y.-J. Tang, P. Gantzel, K. Meyer, *Organometallics* **22** (2003) 612.
- [4] X. Hu, I. Castro-Rodriguez, K. Olsen, K. Meyer, *Organometallics* **23** (2004) 755.
- [5] F.E. Hahn, M.C. Jahnke, *Angew. Chem., Int. Ed.* **47** (2008) 3122.
- [6] X. Hu, K. Meyer, *J. Organomet. Chem.* **690** (2005) 5474.
- [7] O. Einsle, F.A. Tezcan, S.L.A. Andrade, B. Schmid, M. Yoshida, J.B. Howard, D.C. Rees, *Science* **297** (2002) 1696.
- [8] M. Aliaga-Alcalde, S.D. George, B. Mienert, E. Bill, K. Wieghardt, F. Neese, *Angew. Chem., Int. Ed.* **44** (2005) 2908.

- [9] C. Vogel, F.W. Heinemann, J. Sutter, C. Anthon, K. Meyer, *Angew. Chem., Int. Ed.* 47 (2008) 2681.
- [10] J.J. Scepaniak, M.D. Fulton, R.P. Bontchev, E.N. Duesler, M.L. Kirk, J.M. Smith, *J. Am. Chem. Soc.* 130 (2008) 10515.
- [11] J.J. Scepaniak, J.A. Young, R.P. Bontchev, J.M. Smith, *Angew. Chem., Int. Ed.* 48 (2009) 3158.
- [12] K. Ward Jr., *J. Am. Chem. Soc.* 57 (1935) 914.
- [13] A.J. Arduengo, III, F.P. Gentry, Jr., P.K. Taverkera, H.E. Simmons, III, in: U.S. (E. I. Du Pont de Nemours & Co., USA), US, 2001, p. 7.
- [14] SADABS 2.06, Bruker AXS, Inc., Madison, WI, USA, 2002.
- [15] SHELXTL NT 6.12, Bruker AXS, Inc., Madison, WI, USA, 2002.
- [16] F. Neese, ORCA – an Ab Initio, Density Functional and Semiempirical SCF-MO Package, version 2.7 revision 0, Institut für Physikalische und Theoretische Chemie, Universität Bonn, Germany, 2009.
- [17] A.D. Becke, *Phys. Rev. A* 38 (1988) 3098.
- [18] J.P. Perdew, *Phys. Rev. B* 34 (1986) 7406.
- [19] J.P. Perdew, *Phys. Rev. B* 33 (1986) 8822.
- [20] A.D. Becke, *J. Chem. Phys.* 98 (1993) 5648.
- [21] C.T. Lee, W.T. Yang, R.G. Parr, *Phys. Rev. B* 37 (1988) 785.
- [22] P.J. Stephens, F.J. Devlin, C.F. Chabalowski, M.J. Frisch, *J. Phys. Chem.* 98 (1994) 11623.
- [23] A. Schäfer, H. Horn, R. Ahlrichs, *J. Chem. Phys.* 97 (1992) 2571.
- [24] F. Neese, *Inorg. Chim. Acta* 337 (2002) 181.
- [25] S. Sinnecker, L.D. Slep, E. Bill, F. Neese, *Inorg. Chem.* 44 (2005) 2245.
- [26] S. Portmann, MOLEKEL, version 4.3.win32, CSCS/UNI Geneva, Switzerland, 2002.
- [27] X. Hu, K. Meyer, *J. Am. Chem. Soc.* 126 (2004) 16322.
- [28] X. Hu, I. Castro-Rodriguez, K. Meyer, *J. Am. Chem. Soc.* 126 (2004) 13464.
- [29] M. Brookhart, M.L.H. Green, G. Parkin, *Proc. Natl. Acad. Sci.* 104 (2007) 6908.
- [30] P.B. Hitchcock, M.F. Lappert, P. Terreros, *J. Organomet. Chem.* 239 (1982) C26.